AIMS Geosciences

AIMS Geosciences, 11(4): 828–845.
DOI: 10.3934/geosci.2025035
Received: 12 April 2025
Revised: 10 August 2025
Accepted: 01 September 2025
Published: 16 October 2025

https://www.aimspress.com/journal/geosciences

Research article

Full-scale load tests to assess the bearing capacity of peat at Zegveld

J Zhang[1,*], T de Gast[1], C Zwanenburg[1,2] and KG Gavin[1]

[1] Faculty of Civil Engineering and Geosciences, Delft University of Technology, 2628, CN, Delft, the Netherlands
[2] Deltares, P.O. box 177, 2600 MH, Delft, the Netherlands

* **Correspondence:** Email: J.Zhang-20@tudelft.nl; Tel: +31-642931951.

Abstract: Great lengths of railway embankments are constructed on organic clay and peat layers, which are highly susceptible to significant deformations under train loading. The growing demand for transportation necessitates a re-evaluation of the stability of railway embankments constructed on peat. Current national railway stability design codes require the undrained shear strength of soils as a key strength parameter. However, the intrinsic heterogeneity of peat, coupled with the presence of fibres and peat's exceptionally high friction angle, complicates laboratory-scale characterisation. Consequently, full-scale field load tests are increasingly essential as critical benchmarks to validate laboratory findings. This study introduces a method for conducting load tests on peat soil at an instrumented benchmark peatland site in Zegveld, the Netherlands. The site setup is described in detail, and selected results from static load tests and in situ probe tests are presented and correlated. These results are then used to conduct a preliminary analysis of the in situ operational shear strength of the peat layer.

Keywords: organic soil; peat; shear strength; field characterisation; shallow foundation

1. Introduction

Most soft-soil railway embankments in the Netherlands were constructed 100–150 years ago. Over time, the embankments have been widened, and the amount of embankment material has been increased

due to ongoing maintenance. However, train loads have significantly increased over time, necessitating a more precise evaluation of existing bearing capacity evaluation methods to ensure the continued safety of these embankments. The systematic assessment of embankment stability was conducted following the guidelines outlined in ProRail OSV000056-7.1 [1] and RLN00414-1-V001 [2]. The OSV000056-7.1 guideline implicitly incorporates partial safety factors for soil strength and train loading within a semi-probabilistic framework. Similarly, the factor of safety (FS) defined in RLN00414 is used to evaluate embankment stability based on a two-dimensional slip plane analysis, which is typically performed using the limit equilibrium method (LEM). Based on current parameter-based analyses, many operational railway embankments would be classified as having insufficient bearing capacity, implying the need for extensive reinforcement measures. Consequently, an appropriate selection of the input characteristic value of undrained shear strength (s_u) is critical for accurate stability assessments.

The establishment of test sites on soils with representative characteristics enables a more comprehensive assessment of their specific mechanical behaviour while minimising the influence of scaling laws [3,4]. Various soil types exhibit unique challenges that are difficult to fully capture in small-scale laboratory experiments and require field-scale tests. For instance, sand is subjected to cementation and ageing effects [5], quick clay exhibits high sensitivity [6], and silt behaviour is strongly influenced by drainage conditions [7]. In the case of peat soil, several factors complicate conventional laboratory and in situ shear strength testing. These include its inherently low strength, the influence of end restraint effects, potential rate-dependent behaviour, and the presence of fibrous inclusions, all of which hinder reliable interpretation of test results [8–10]. Furthermore, field probe tests are highly sensitive to instrument accuracy, temperature variations, and partial drainage conditions, introducing additional uncertainties [11,12]. Given these complexities, strength and stiffness parameters obtained through back-analysis of full-scale field tests are considered the most reliable, as they are less affected by sampling disturbance and scaling effects [13,14]. Multiple studies underscore the importance of representative field test sites combined with high-quality in situ and laboratory investigations to realistically characterise soil behaviour under conditions that are difficult to replicate in standard testing environments [15–17]. This underscores the need for full-scale field investigations on peat sites, providing benchmark values for advancing the understanding and modelling of peat behaviour in engineering applications.

To address the mentioned challenges in peat characterisation, a series of full-scale load tests was designed and conducted on the peatland in Zegveld. This paper provides a detailed description of the overall test site setup and presents selected results from the load tests and in situ probe tests. These results are used to assess the operational shear strength of peat under field conditions. The paper also discusses the potential applications of the subsequent test results.

2. Characterisation of the peat at the test site and the load apparatus

The experimental farm near the village of Zegveld is managed by Kennis Transfer Centrum (KTC) Zegveld and is located in the western Netherlands (Figure 1a). The farm is situated within a typical peat meadow landscape and serves as a monitoring site for the anticipated increase in land subsidence due to lowered ditch water levels.

The soil profile at Zegveld primarily consists of eutrophic wood-sedge peat (*Carex* and *Alnus*), underlain by Pleistocene sand at approximately 6 m below the surface [18]. The organic matter content in the 0–30 cm surface layer ranges from 50% to 70% by weight, gradually increasing to 80%–85% at a depth of 80 cm as the degree of decomposition decreases. Wood remains are most abundant in the upper 3 m of the profile, while the peat predominantly comprises sedge and reed below this depth. Figure 2a presents a representative borehole log from the test site, showing a relatively uniform peat layer approximately 6 m thick, starting from 30 cm below the ground surface. Figure 2b shows a sample of wood remnants retrieved from a depth of 1 m within the peat. The wood structure was poorly preserved and difficult to distinguish, and muddy water without fibrous peat was extruded during hand-squeezing. The peat exhibited a high wood content, with only a small amount of coarse fibres present and an absence of fine fibres. Upon exposure, the peat emitted a distinct smell. Based on laboratory observations and following the extended von Post classification system proposed by Hobbs [19,20], the peat at this depth is approximately classified as $H_4B_3F_0R_1W_3N_3A_2$.

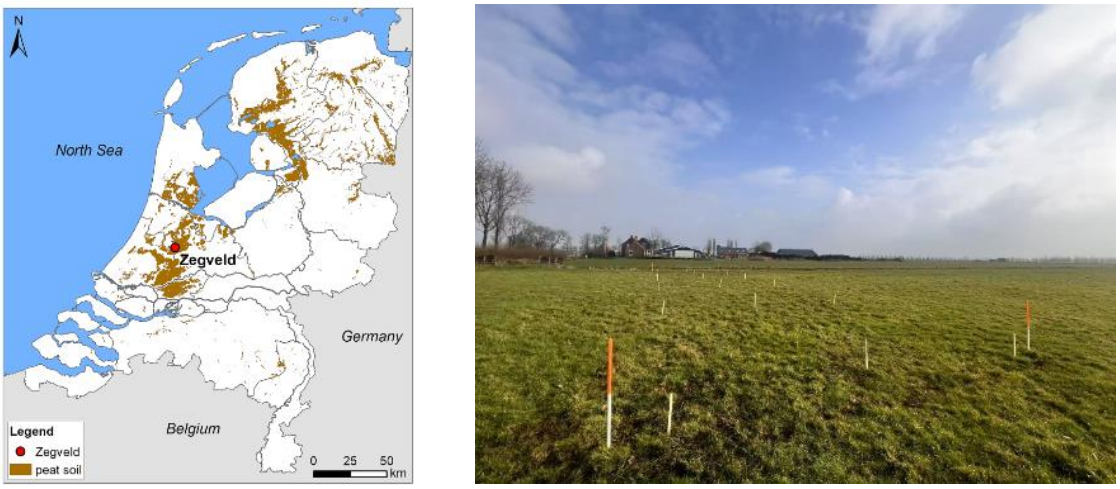

(a) (b)

Figure 1. (a) Location of Zegveld test site. Adapted from [20]. (b) Site photograph (sticks mark excavation and CPT locations).

Figures 3a–c presents the laboratory results of saturated unit weight (γ_{wet}), water content (w), and loss on ignition (LOI) at the test site [21]. Notably, the average saturated unit weight is only 9.90 kN/m³, which is only slightly higher than the density of water. Given the high groundwater table at the site, this results in extremely low effective stress levels in the peat soil—an observation that is typical for such environments. Incremental loading (IL) oedometer tests were performed on seven samples taken from depths between 0.50 and 1.52 m below the ground surface. A series of successive loading steps, ranging from 2 to 140 kPa, was applied. Figure 3d illustrates the results of one representative incremental loading test on a sample taken from 0.50 m [22]. The preconsolidation stress (P_c), was determined using the Casagrande method [23]; for the seven tests, it ranged from 9.0 to 15.4 kPa, while the initial void ratio (e_0) varied between 8.32 and 12.77.

Figure 2. (a) Typical borehole log (b) wood remnants from peat at 1 m depth below the surface.

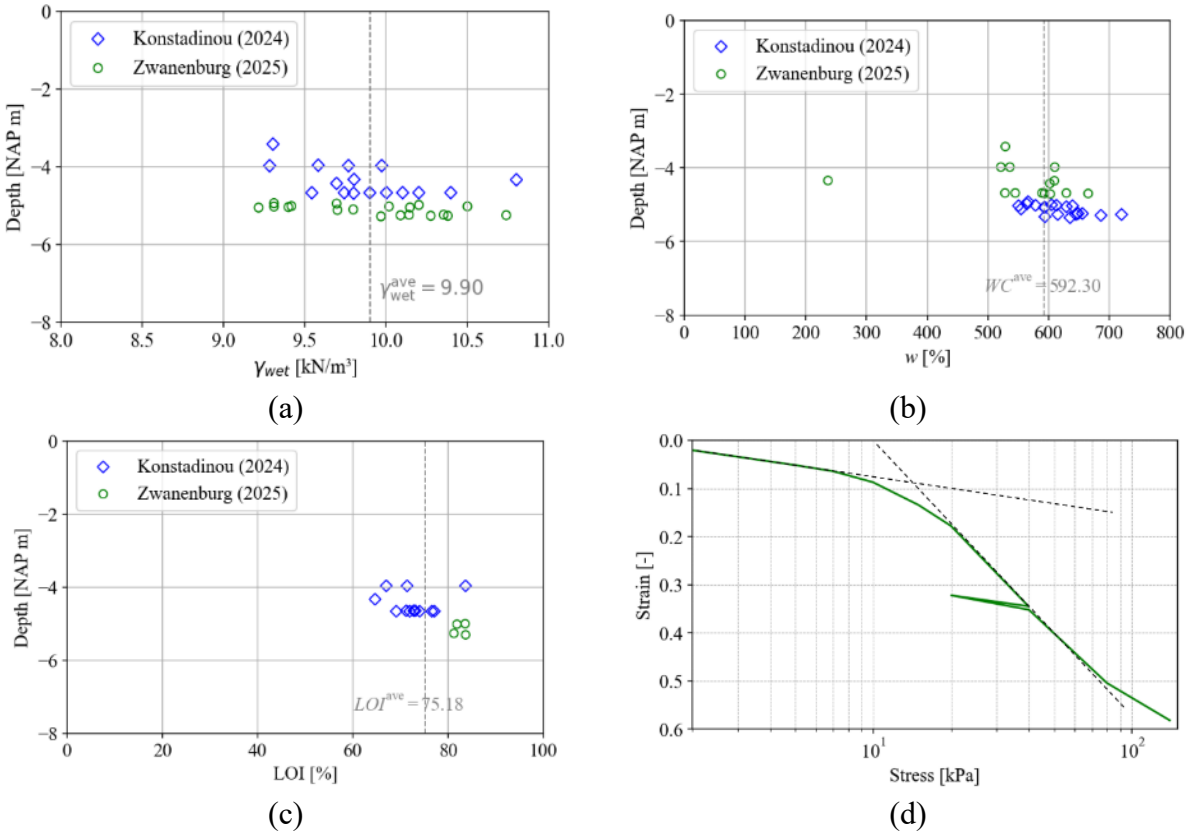

Figure 3. Soil profile of (a) saturated unit weight (γ_{wet}) (b) water content (w), and (c) loss on ignition (LOI). (d) Linear strain as a function of stress, incremental loading oedometer test.

Figure 4a compares the relationship between the initial void ratio and initial water content of the IL test sample, as well as with peat and organic clay from several other sites in the Netherlands. It can be seen that the overall trend fits well, and the initial void ratio of the Zegveld peat is lower than that of Uitdam. Figure 4b illustrates the relationship between the coefficient of permeability (k) and void ratio (e_0), obtained from the incremental loading oedometer test presented in Figure 3d, in comparison with data from other soil types and published peat datasets [10,24,25]. The permeability was determined using the Casagrande method [26,27]. The results are observed to lie within the characteristic range of k values reported for peat soils.

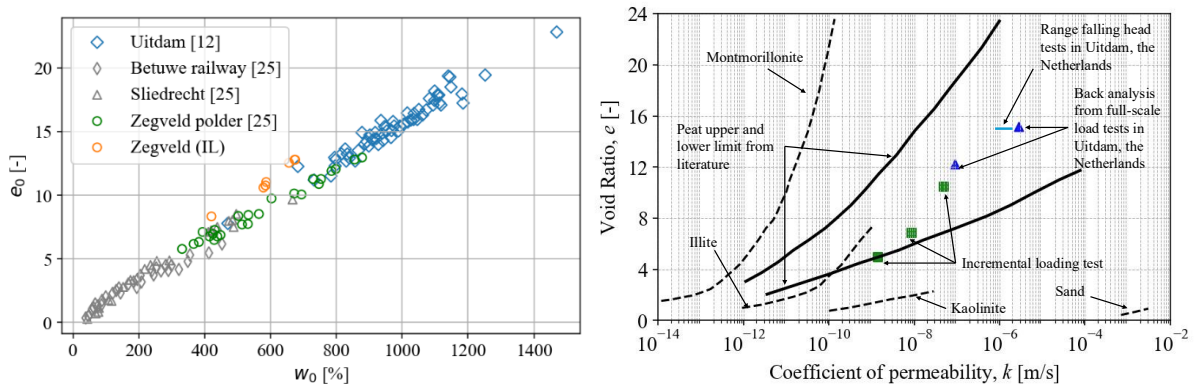

(a) (b)

Figure 4. (a) Relation between void ratio, e_0, and water content (w). (b) Permeability measured from the laboratory incremental loading test, compared with the back analysis from full-scale tests [12], upper and lower limits of peat, and other types of soil from [26].

The loading apparatus used in the tests is shown in Figure 5a. The applied load was generated by a vertical seismic vibrator (e-vib) [28] in combination with its supporting structure. The supporting structure consisted of a 2000 mm × 2000 mm supporting plate that carried the e-vib, which was connected via two conical connectors to a circular loading plate with a diameter of 500 mm. The structure was instrumented with a load cell and three laser optical displacement sensors to monitor the applied force on the loading plate and the vertical displacement of the system during loading. When in operation, the vibrator transmitted cyclic loading to the loading plate. When inactive, a crane system was employed to apply static loading in incremental steps.

The test site is located in the northwest corner of the farm. As shown in Figure 6a, a total of 11 cyclic load tests and 9 static load tests were conducted. Before testing, an excavation was carried out to remove the surface layer of anthropogenically disturbed soil and expose the underlying peat layer. The excavation measured 1.5 × 1.5 m in area and 1.0 m in depth (0.5 m for the static test 2 and 1.5 m for the static/cyclic test 3). A flat bottom surface was organised to facilitate loading after excavation. Both the cyclic and static loading tests were conducted within the same excavation, positioned at opposite corners. Before excavation, a total of 12 cone penetration tests (CPT) and 6 ball penetrometer tests were conducted. The tests were arranged in three rows, with a spacing of 3.5 m between rows and 6 m between individual probe locations within each row. The CPTs were positioned near the edges of

each planned excavation area. After the completion of the load tests, the excavations were backfilled with in situ soil. Subsequently, an additional 12 CPTs were carried out; 10 were conducted at the locations where cyclic load tests had been carried out, and the remaining 2 were conducted at the locations of static load tests.

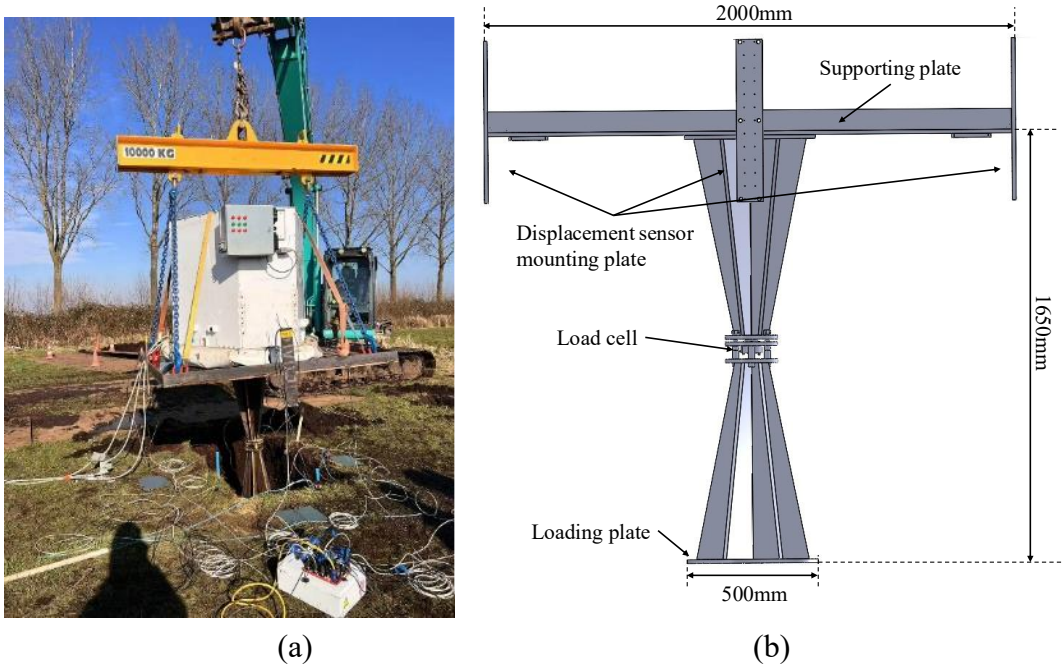

Figure 5. (a) The load apparatus deployed in the test site. (b) Supporting structure.

This paper selects the results of static load tests 8 and 9, with the instrumentation layout shown in Figure 6b. Three pore pressure transducers (PPT) were installed directly beneath the loading plate, and an additional transducer was positioned adjacent to the plate. Furthermore, two total stress transducers (TST) were placed beneath the plate. The installation depth for both the PPTs and the TSTs beneath the plate was 0.3 m below the excavation surface, while the PPT located outside the plate was installed at a depth of 0.5 m.

3. Field probe test

Figure 7a–c presents the pre-test CPT results at test 8 and test 9 locations. The corrected cone resistance, q_{net}, was derived from [29]:

$$q_{net} = q_c + (1-a)u_2 - \sigma_{v0} \quad (1)$$

in which q_c represents the uncorrected cone resistance, a is the cone area ratio (0.75 here), u_2 is the pore pressure measured above the cone shoulder, and σ_{v0} is the overburden pressure. Figure 7a shows ~0.5 m depth dry crust at the surface, followed by a 0.1–0.2 MPa value within the depth range of −3.5 to −8.8 m NAP; both CPTs exhibit nearly constant q_{net} values, with only minor fluctuations. Based on

fitting the values within the intermediate depth range, the representative q_{net} values for test 8 and test 9 were determined to be 206.2 and 164.5 kPa, respectively.

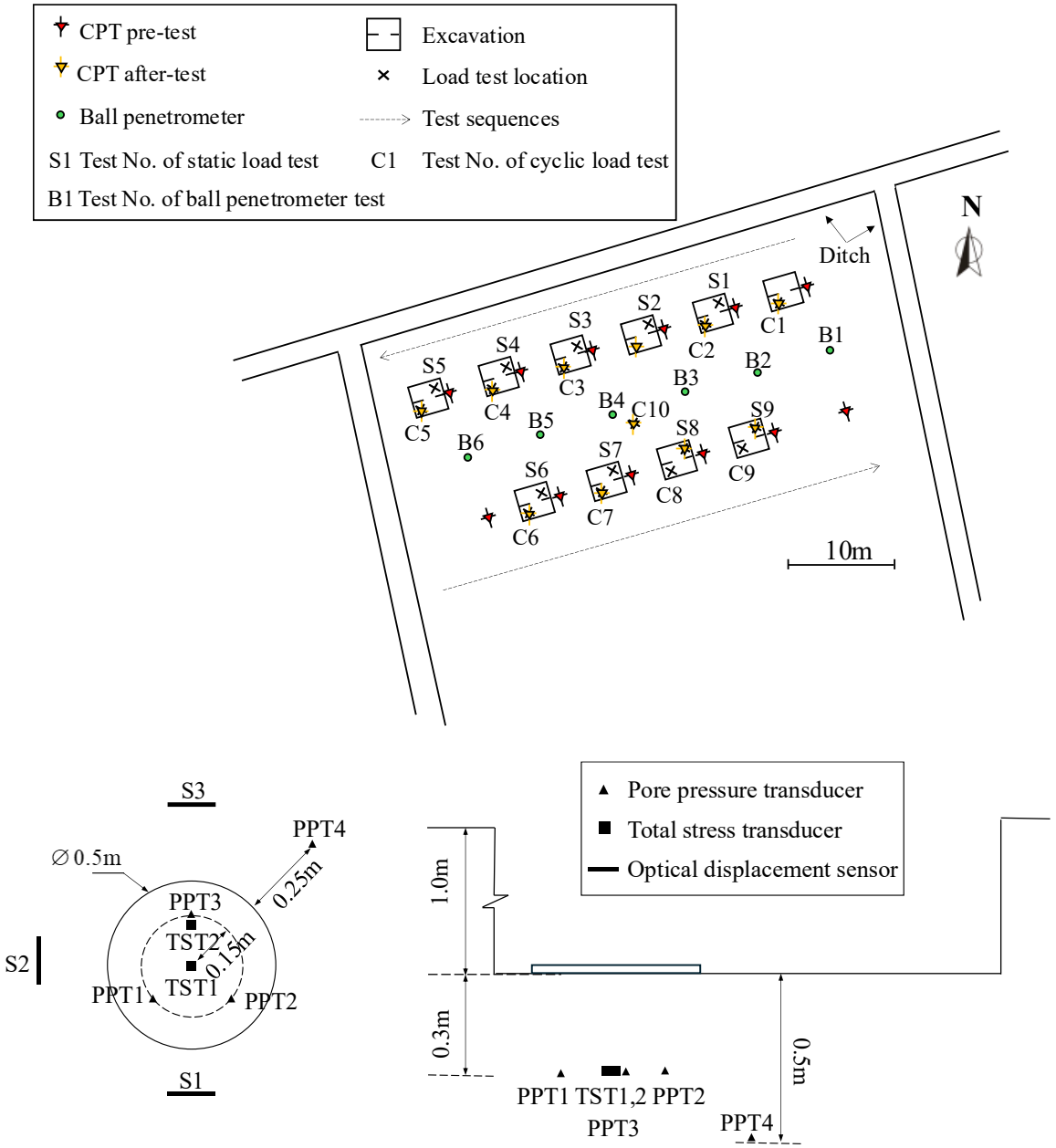

(b)

Figure 6. (a) Test site overview. (b) Instrumentation of test 8 and test 9.

As shown in Figure 7b, the friction ratio (R_f) of both CPTs increases and reached a maximum value of 25%. At approximately 3 m below the surface (NAP: 6 m), the R_f value drops to around 5% and then remains relatively stable until reaching the sand layer. Differences in Rf values within peat layers may indicate variations in peat type with depth. Figure 7c shows the measured pore water pressure profile and the hydrostatic line. Notably, negative pore water pressure values were recorded in the upper soil layers. This phenomenon can be attributed to the lateral displacement of the soil combined with tensioning of

the horizontal fibres during penetration [21]. These result in a localised increase in pore volume, which leads to a reduction in pore water pressure, u_0. The rate of water inflow into the expanding pore is insufficient to maintain hydrostatic equilibrium during penetration, thereby generating negative excess pore pressures at the cone shoulder. Figure 7d shows the profile of the pore water pressure ratio, B_q:

$$B_q = \frac{u_2 - u_0}{q_{\text{net}}} \tag{2}$$

The negative value of u_2 led to a negative B_q at the initial stage of penetration. As the depth increased, the B_q value returned to positive starting from NAP −6 m, and fluctuated around 0.1 between NAP −7 m and −9 m. Upon entering the sand layer, it quickly returned to around 0.

Figure 7e shows the results from the two ball penetrometer tests conducted closest to the load test area. The ball penetrometer data did not require any correction; nevertheless, the measured q_{ball} values showed smaller fluctuations compared to q_{net}.

The soil behaviour type (SBT) classification results based on CPT are presented in Figure 7f. Considering the insensitivity of the Robertson (2010) SBT classification chart [30] in distinguishing between organic clays and mineral clays, an updated classification method tailored for Dutch peat and organic clays based on the Robertson SBT was adopted [31]. Based on the combined results from Figures 7a–e, a uniformly distributed peat and organic clay layer, approximately 6 m in situ thick, is observed at both test sites. This layer is underlain by a thin clay stratum, which transitions into sand at greater depths. These observations are generally consistent with the description by Massop et al. [20], who reported that the upper 3 m of peat are rich in woody material, while the deeper sections consist primarily of sedge and reed peat. However, the classification results from test 8 indicate the presence of a clay and silt mixtures layer between 5.6 and 5.9 m, as well as interbedded organic clay layers throughout the peat layer. The clay layer is reflected in Figures 7a–c, while the presence of interbedded organic clays may be due to the ambiguity in differentiating between peat and organic clay in the classification method. Considering the low q_c values measured in the peat layer, which approach the minimum accuracy of CPT [32], a sensitivity analysis was conducted by increasing and decreasing q_c values by 0.025 MPa. The results show that decreasing q_c led to a more uniform peat layer in both tests, whereas increasing q_c resulted in a higher proportion of the layer being classified as organic clay. Nevertheless, the clay and silt mixtures layerin test 8 remained consistently identified.

4. Load test

To demonstrate the capacity of the loading system, the monitoring results from static load tests 8 and 9 were selected for analysis. The sensor layout is shown in Figure 6b. The results of the static load test are presented in Figures 8 and 9. Figure 8a shows the applied stress from the load cell reading. Under crane control, the stress was applied to the loading plate incrementally by releasing it in stages, with each stage corresponding to approximately 12.5 kPa. Once the target load was reached, the crane stopped releasing additional weight. After the stress reached a peak value of 75 kPa, the loading system was held for approximately 100 seconds to observe the dissipation of excess pore pressure. Eventually, when stress was increased further to 93 kPa, the soil could no longer provide sufficient bearing capacity, even with

additional loading. It was also observed that after each rapid loading increment, the applied load exhibited a slight decrease, while the soil stabilised following an initial phase of rapid settlement. This might be attributed to the stop of the loading plate controlled by the crane boom, which induces a stress relaxation adjustment of the soil at the contact interface.

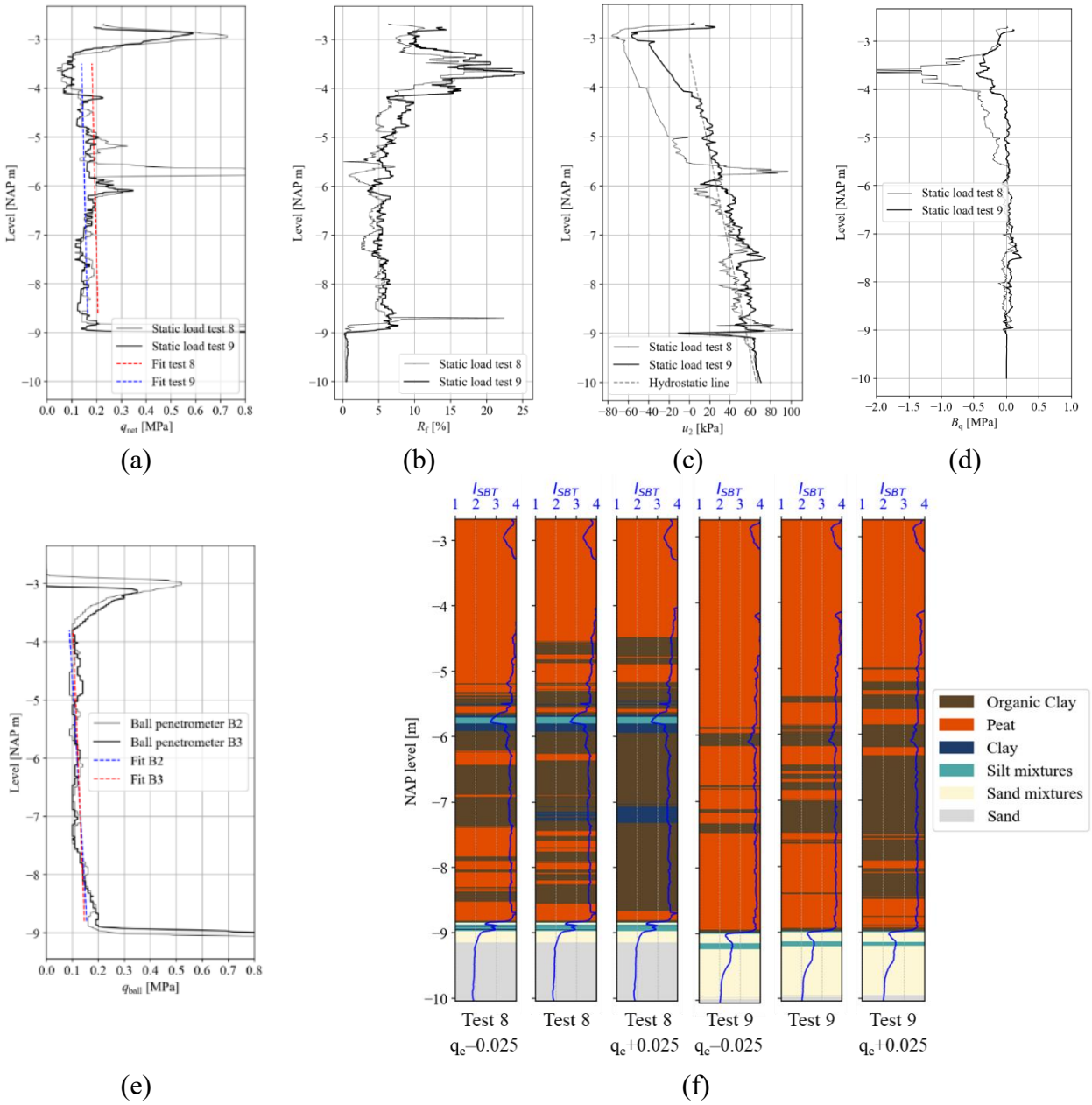

Figure 7. Pre-test CPT profiles for static load tests 8 and 9: (a) corrected cone resistance qnet, (b) friction ratio, R_f, and (c) pore pressure measured at the shoulder of the cone, u_2. (d) Pore water pressure ratio. B_q (e) ball penetrometer resistance, q_{ball} (e) SBT classifications.

As shown in Figure 8b, the settlement at each loading step increased progressively with the applied stress. When the final stress was increased to 93 kPa, a sudden settlement and tilting of the

entire loading structure were observed. According to the results from the three displacement sensors, the structure tilted in the direction of Laser 3. During this loading stage, the average soil settlement reached approximately 300 mm, with a maximum recorded settlement of 410 mm.

Figure 8c shows that both total stress and excess pore pressure increased correspondingly with each load increment. Compared to TST2, TST1, located at the centre of the loading area, exhibited greater increases at each loading step. A drop in total stress readings was observed after each loading stage, consistent with the unloading effect caused by crane braking as discussed in Figure 8a. The increase in pore water pressure closely mirrored that of the total stress, indicating that the instantaneous load was almost entirely converted into excess pore pressure. Notably, the drop in pore pressure after unloading closely matched the drop in total stress, suggesting that the decrease in pore pressure following each load step was primarily due to unloading rather than dissipation. During the final loading stage, TST1 recorded the highest peak total stress at 44 kPa. On the side of the loading plate facing Laser 3, PPT3 exhibited the highest excess pore pressure, peaking at 29 kPa. In contrast, the increases in PPT1 and PPT2 were smaller, which is likely attributable to the effects of non-uniform settlement. PPT4, located outside the loading plate, was less affected by unloading and showed a steady, stepwise accumulation of pore pressure until failure.

Figure 9 presents the results of static load test 9, which followed a loading trend similar to that observed in test 8 (Figure 8). In Figure 9a, the applied stress was successfully increased to 61 kPa; however, when an attempt was made to increase it further, the reading only reached 69 kPa before rapidly declining. Subsequent loading attempts indicated that the soil could no longer provide sufficient bearing capacity. Figure 9b illustrates the settlement of the entire loading system as the applied load increased. Initially, the settlement increased progressively and stabilised until stress reached 61 kPa. When stress was increased beyond this point, the soil exhibited a sudden settlement of nearly 40 mm, prompting intervention with the crane boom to prevent excessive sinking. A slight tilting of the structure toward the direction of Laser 2 was observed at this stage. A subsequent release of the load resulted in an average observed settlement of 110 mm, while the tilting of the structure remained evident. Figure 9c shows the response of total stress and pore water pressure, which is similar to the trends observed in Figure 8c. During the final loading stage, PPT1, located on the side of Laser 2, recorded a peak excess pore pressure of 43 kPa. However, TST2 and PPT3, which were installed in nearby positions, although responsive to each loading increment, exhibited significantly lower increases compared to other sensors. Considering the heterogeneity of the peat at the installation locations, particularly the presence of incompletely decomposed plant material, it is hypothesised that fibrous structures in the vicinity of these sensors may have absorbed part of the stress transfer, thereby attenuating the measured response.

5. Discussion and assessment of the peat strength

Peat strength is characterised based on the results of in situ probing and load tests. In accordance with Dutch standards for macro-stability analysis, peat is treated as undrained in ultimate limit state calculations, and the undrained shear strength, s_u is introduced via the SHANSEP method [33]. However, due to the open structure of peat and the possible presence of gas, even short-term loadings may occur

under partially drained conditions, and ideal undrained behaviour may not be achieved. Nevertheless, for macro-stability analyses, using undrained shear strength generally yields more accurate and conservative results than using drained strength, and this approximation is widely accepted. In the discussion that follows, drainage conditions in probing and load tests are discussed by calculating the normalised penetration rate, V, and the degree of consolidation, U, respectively. The aim is to demonstrate that the results can be used to parameterise calculations within the undrained framework. However, acknowledging the partial drainage under field conditions, the term "strength from investigation methods" instead of "undrained shear strength" is adopted in the following description.

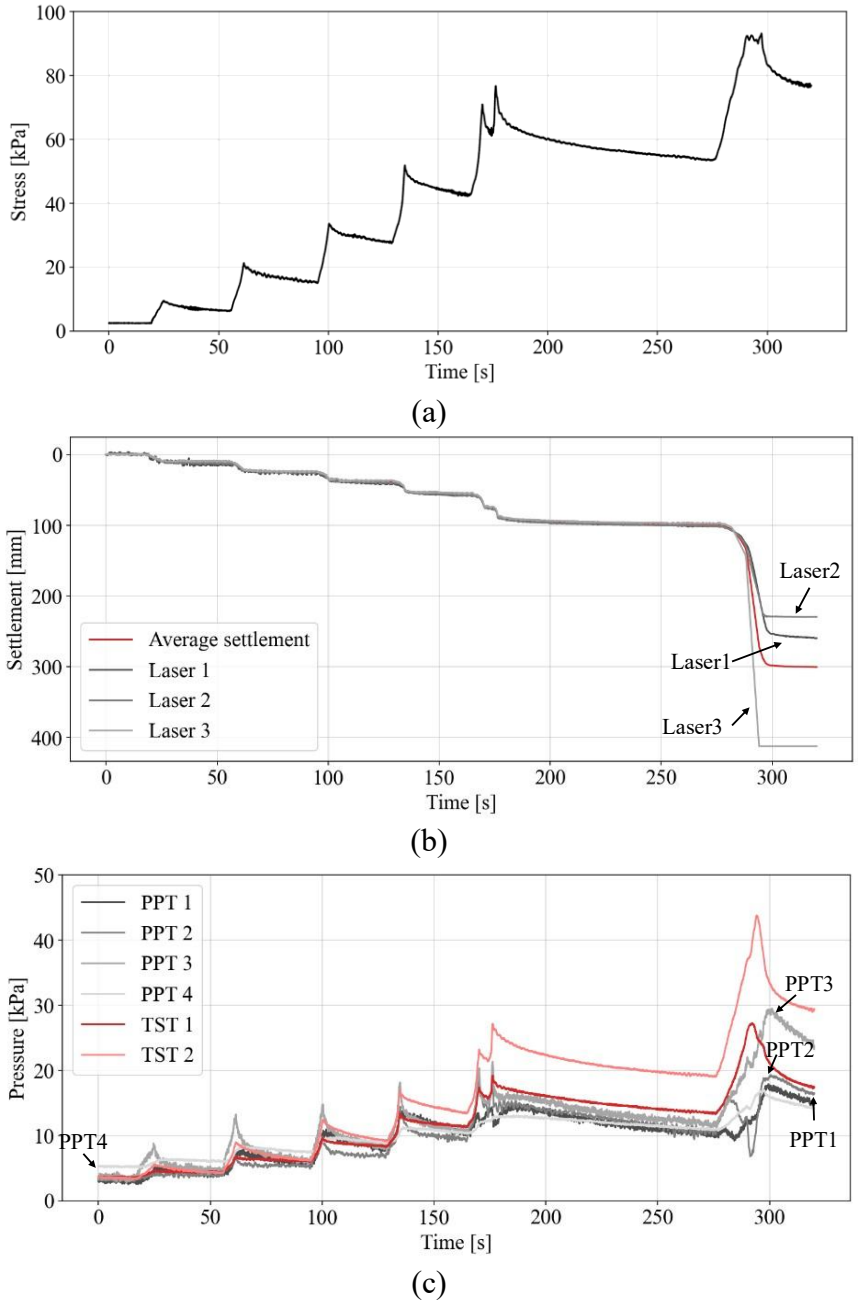

Figure 8. (a) Loading, (b) settlement, and (c) pore water pressure and total stress with time in the static load test 8.

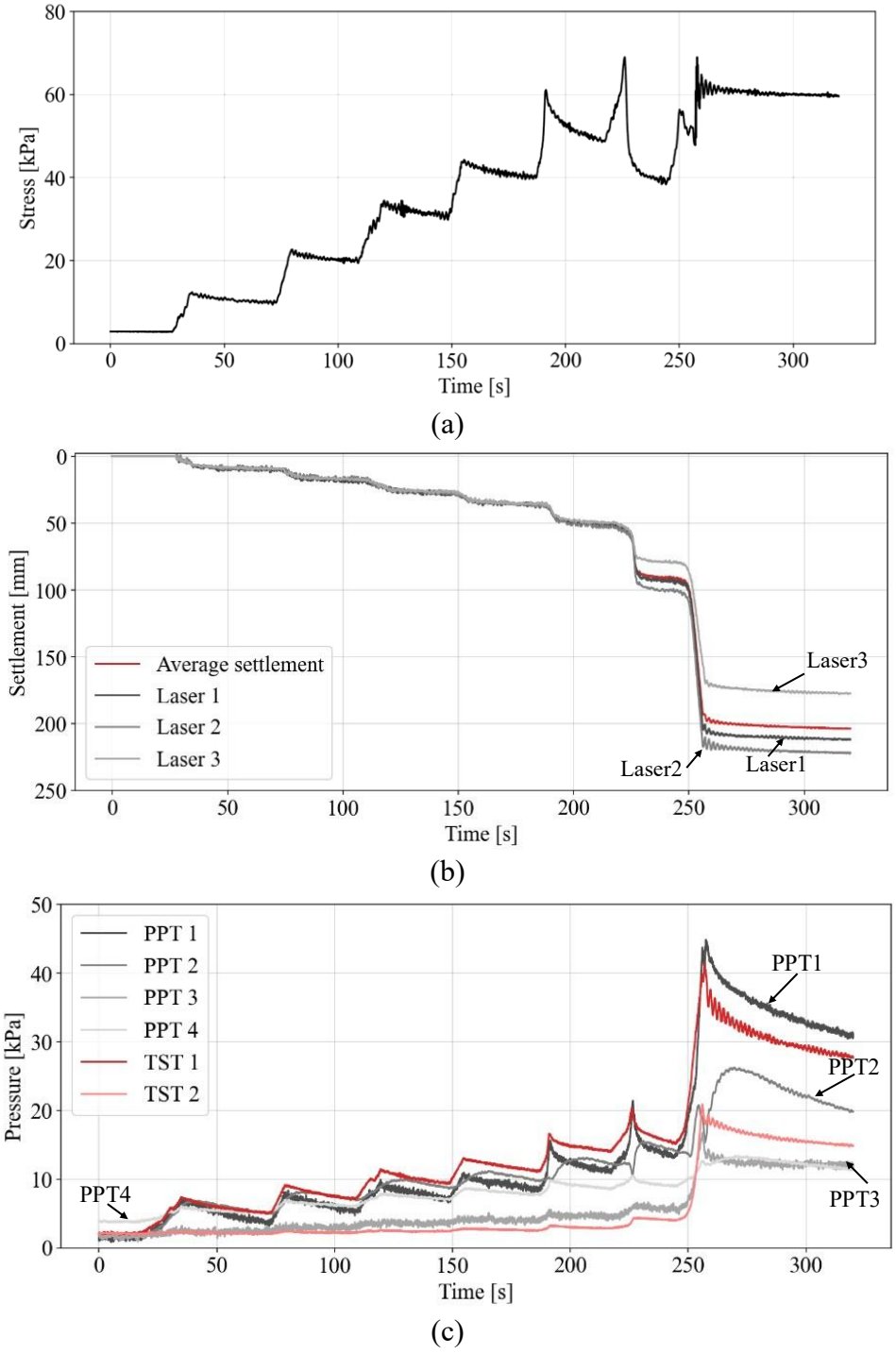

Figure 9. (a) Loading, (b) settlement, and (c) pore water pressure and total stress with time in the static load test 9.

For peat soils, correlating results from probe tests and field loading tests with the strength requires careful consideration of drainage conditions. For probe tests [34]:

$$V = \frac{vd}{c_v} \tag{3}$$

In which v is the penetration velocity (0.02m/s), d is the probe diameter, and c_v is the coefficient of consolidation. The c_v is derived from the first loading step of the oedometer test in Section 2, during

which the void ratio decreases from an initial value of 11.03 to 10.76 after consolidation. The calculated c_v is approximately 47.3 m²/year (Table 1).

Undrained behaviour is expected when the value of V exceeds 30–100 [34], while drained behaviour typically occurs when V is below 0.01. The calculated V values for both cone and ball penetrometers are clearly above this threshold, suggesting that the soil surrounding the penetrometer behaves in an undrained condition. However, based on the profiles shown in Figure 7c and 7d, it can be inferred that partial drainage may occur in the peat. When using CPT data to estimate the shear strength of peat, penetration at the standard rate does not necessarily occur under fully undrained conditions. It should be noted that the failure mechanism during CPT penetration in peat differs from that in clays, which are commonly used to interpret CPT-based strength [35]. Nevertheless, extensive field CPT results have shown promising correlations with peat shear strength [8,10,12]. Therefore, CPT results in peat are correlated with undrained shear strength for stability assessment, despite the complexity of drainage conditions within the peat during the penetration process.

Table 1. Normalised penetration velocity, V.

Probe	D [m]	V [-]
		c_v = 47.3 m²/year (1.5×10^{-6} m²/s)
Cone, 10 cm²	0.0357	476
Ball, 100 cm²	0.115	1533

For the estimation of drainage conditions during the loading tests, it is important to note that due to the limited size of the loading plate and the nature of peat, both vertical and horizontal drainage can occur. In particular, the horizontal permeability may be 3–5 times greater than the vertical permeability [25]. Consequently, the use of Terzaghi's one-dimensional consolidation theory is inadequate to accurately represent the consolidation rate in this condition [36]. Instead, a consolidation analysis based on Biot's theory [37] is considered, specifically for a circular footing resting on a finite stratum [38]. This approach allows for the inclusion of three-dimensional consolidation effects and the stratum thickness. For the case of a permeable base, the dimensionless time factor (T_p) can be expressed as

$$T_p = (0.715\nu^2 - 2\nu + 1.4533)\left\{\alpha + \left[6 + 100\left(\frac{h}{H}\right)^{9/4}\right]\left(\frac{r_0}{H}\right)^{9/4}\right\}\frac{C_{v3}t}{H^2}, C_{v3} = \frac{kE}{3\gamma_w(1-2\nu)} \quad (4)$$

In which h and H are the embedded depth and thickness of the soil stratum, respectively. α is a function of h/H, and r_0 is the radius of the circular footing. C_{v3} is the coefficient of consolidation under three-dimensional strain conditions. E and ν are the Young's modulus and Poisson's ratio, respectively. γ_w is the unit weight of water.

Based on site conditions, the thickness of the peat layer is H = 6, and the embedded depth corresponds to the excavation depth h = 1 m, giving a ratio of h/H = 0.167. Referring to relevant charts in [36], this corresponds to a α of 2.12. Using back-analysis results from similar in situ tests on peat, the Young's modulus is taken as E = 500 kPa, and the Poisson's ratio as v = 0.15 [12]. The coefficient of permeability k is taken as the maximum value calculated from the incremental loading test, 5.02 ×

10^{-8} m/s. From these values, the dimensionless time factor is computed as $T_p = 2.52 \times 10^{-5}$, which corresponds to a degree of consolidation $U < 5\%$ based on solution charts. This indicates that the loading test can reasonably be considered to have occurred under approximately undrained conditions. It is important to note that in the estimation of drainage conditions for both the probe and loading tests, the input values for the coefficient of consolidation, c_v, and coefficient of permeability, k, were based on the maximum permeability obtained from the laboratory incremental loading tests. As shown in Figure 4, all measured values fall within the typical range for peat permeability, supporting the validity of the predicted results. Additionally, the excess pore pressure accumulation curve recorded by PPT4, located outside the influence zone of crane-induced unloading, also indicates that the tests can be treated as undrained conditions.

Figure 4 further shows that the permeability values obtained from the laboratory tests are lower than those measured at another field site, Uitdam [14]. This discrepancy between field and laboratory permeability values may be attributed to structural features of the peat in situ, particularly the presence of large pores and gas bubbles. The large pore structure in the peat may dominate field drainage behaviour and result in higher in situ permeability. In contrast, the presence of gas bubbles in the field could also slow down the drainage to some extent.

Based on the above discussion, the strength from CPTu and ball penetrometer readings is given by

$$s_u^{CPTu} = \frac{q_{net}}{N_{kt}}, s_u^{ball} = \frac{q_{ball}}{N_b} \tag{5}$$

Within the depth range of −3.5 to −8.8 m NAP, both CPTs exhibit nearly constant q_{net} values, with only minor fluctuations. Based on fitting the values within the intermediate depth range, the representative q_{net} values for test 8 and test 9 were determined to be 206.2 and 164.5 kPa, respectively. For q_{ball}, representative values for B02 and B03 were 124.1 and 122.1 kPa, respectively. For peat soils, a typical value of the cone factor N_{kt} is approximately 15.3, and for N_b is 16.5 [12]. Using these factors, the estimated strengths from CPT data s_u^{CPTu} are 13.5 kPa for test 8 and 10.8 kPa for test 9. The corresponding strengths derived from ball penetrometer tests s_u^{ball} are 7.5 kPa for B02 and 7.4 kPa for B03.

The results from the ball penetrometer reflect the spatial variability of peat strength in the field, as their test locations differ from those of the load tests. Therefore, they are not used for direct comparison with the loading test data.

Based on the loading curves from tests 8 and 9, the soil was observed to reach failure when the applied stress on the loading plate reached 93 and 69 kPa, respectively. These correspond to ultimate bearing capacities, q_u. In classical bearing capacity theory, the bearing capacity factor N_c relates the surface failure load q_u to the strength from static load test s_u^{sl} and can be expressed as [39]:

$$N_c = \frac{q_u}{s_u^{sl}} \tag{6}$$

Using the strengths derived from CPT data, the bearing capacity factors N_c for static load tests 8 and 9 were calculated to be 66.89 and 6.39, respectively. The values show good reproducibility of the tests. These values are slightly higher than the theoretical value of 6.05 [40] typically adopted for

circular footings on undrained materials. This discrepancy is attributed to the influence of the vertical excavation sidewalls, which provide additional confinement and enhance the bearing capacity.

6. Conclusions

This paper presented the design of the loading tests conducted at the Zegveld peatland site and provided preliminary results from selected static loading and probe tests. The drainage conditions of the probe and loading tests were evaluated using empirical formulas and solution charts. It was determined that both the penetration and loading processes could be considered undrained ($V > 100$, $U < 5\%$), supporting the feasibility of correlating the results to undrained shear strength. However, due to the existence of air bubbles and the discrepancies between laboratory-derived and field-measured permeability, it remains complex to conclusively determine the actual drainage conditions during testing. Further analysis involving the back-calculation of pore pressure dissipation after the loading tests could help to more reliably estimate the in situ coefficient of consolidation. The strength derived from CPT data was used to assess the bearing capacity observed in the loading tests. Both tests got consistent bearing capacity factors, demonstrating the potential reliability of CPT-based strength evaluation in peat. However, given the inherent heterogeneity and rate dependency of peat, further validation through additional testing is required to confirm this relationship.

It is also worth noting that the loading system used in this study is capable of applying sinusoidal cyclic loading. The results of the cyclic loading tests are subject to further analysis and will be published elsewhere. The objective of this loading method is not to directly replicate train-induced loading on the subsoil of railway embankments but rather to investigate the behaviour of peat under cyclic loading within an independent boundary condition. The findings from these tests will be further utilised for several key analyses:

1. Characterisation of mobilised strength of peat based on static load test results.

2. Determination of the relationship between bearing capacities under static and cyclic loading, as well as the potential ultimate cyclic stress ratio, through a combined analysis of static and cyclic loading results.

Additionally, samples retrieved from the site will undergo a series of laboratory tests for comparison with previous laboratory findings using the sample from Zegveld [27], in conjunction with results from field tests, which will provide a reference for selecting appropriate parameters for constitutive modelling. The applicability of these constitutive models under different boundary conditions will be further validated using the recorded field data. The results of this study will enhance the understanding of peat behaviour under cyclic loading, leading to more accurate evaluations of ultimate bearing capacity and settlement behaviour for railway embankments constructed on peat layers.

Author contributions

Jiarui Zhang: Writing—original draft, Writing—review & editing, Conceptualization, Formal analysis, Investigation, Data curation, Visualization; Tom de Gast: Writing—review & editing, Formal analysis, Methodology, Investigation; Cor Zwanenburg: Writing—review & editing, Validation,

Methodology, Investigation; Ken Gavin: Writing—review & editing, Methodology, Resources, Project administration.

Use of AI tools declaration

The authors declare they have not used Artificial Intelligence (AI) tools in the creation of this article.

Acknowledgements

The authors acknowledge the ProRail and research program RESET for financing the field tests. Thanks to colleagues from TU Delft and Deltares for their help in assembling the loading system and testing the sensors. Thanks to Arny Lengkeek for helping to verify and correct the SBT classification results.

Conflict of interest

The authors declare no conflict of interest.

References

1. Prorail, Ontwerpvoorschrift—Baanlichaam en Geotechniek. OVS00056-7.1. Dutch. 2016. Available from: https://www.prorail.nl/.
2. Prorail, Richtlijn—Beoordelen constructieve veiligheid bestaande Baanlichamen. RLN00414-1. Dutch. 2016. Available from: https://www.prorail.nl/.
3. Gavin K, Adekunte A, O'Kelly B (2009) A field investigation of vertical footing response on sand. *Proc Inst Civ Eng—Geotech Eng* 162: 257–267. https://doi.org/10.1680/geng.2009.162.5.257
4. de Gast T (2019) *Dykes and embankments: a geostatistical analysis of soft terrain*, PhD Thesis. Delft University of Technology.
5. Gavin K, Igoe D (2021) A field investigation into the mechanisms of pile ageing in sand. *Géotechnique* 71: 120–131. https://doi.org/10.1680/jgeot.18.P.235
6. L'Heureux J-S, Lindgård A, Emdal A, et al. (2019) The Tiller-Flotten research site: Geotechnical characterisation of a very sensitive clay deposit. *AIMS Geosci* 5: 831–867. https://doi.org/10.3934/geosci.2019.4.831
7. Blaker Ø, Carroll R, Paniagua P, et al. (2019) Halden research site: geotechnical characterisation of a post glacial silt. *AIMS Geosci* 5: 184–234. https://doi.org/10.3934/geosci.2019.2.184
8. Boylan N, Long M, Mathijssen FAJM (2011) In situ strength characterisation of peat and organic soil using full-flow penetrometers. *Can Geotech J* 48: 1085–1099. https://doi.org/10.1139/t11-023

9. Muraro S, Jommi C (2021) Experimental determination of the shear strength of peat from standard undrained triaxial tests: correcting for the effects of end restraint. *Géotechnique* 71: 76–87. https://doi.org/10.1680/jgeot.18.P.346
10. Zwanenburg C, Jardine RJ (2015) Laboratory, in situ and full-scale load tests to assess flood embankment stability on peat. *Géotechnique* 65: 309–326. https://doi.org/10.1680/geot.14.P.257
11. Long M, Boylan N (2012) In Situ Testing of Peat—a Review and Update on Recent Developments. *Geotech Eng J SEAGS AGSSEA* 43: 41–55. https://doi.org/10.14456/seagj.2012.5
12. Zwanenburg C, Erkens G (2019) Uitdam, the Netherlands: test site for soft fibrous peat. *AIMS Geosci* 5: 804–830. https://doi.org/10.3934/geosci.2019.4.804
13. Zwanenburg C, Den Haan EJ, Kruse GAM, et al. (2012) Failure of a trial embankment on peat in Booneschans, the Netherlands. *Géotechnique* 62: 479–490. https://doi.org/10.1680/geot.9.P.094
14. Lehtonen VJ, Meehan CL, Länsivaara TT, et al. (2015) Full-scale embankment failure test under simulated train loading. *Géotechnique* 65: 961–974. https://doi.org/10.1680/jgeot.14.P.100
15. Simonini P, Mangraviti V (2025) Comprehensive analysis of test sites for soil stiffness characterisation in the Venice lagoon. *AIMS Geosci* 11: 298–317. https://doi.org/10.3934/geosci.2025013
16. Viana da Fonseca A, Ferreira C, Ramos C, et al. (2019) The geotechnical test site in the greater Lisbon area for liquefaction characterisation and sample quality control of cohesionless soils. *AIMS Geosci* 5: 325–343. https://doi.org/10.3934/geosci.2019.2.325
17. Pineda JA, Kelly RB, Suwal L, et al. (2019) The Ballina soft soil Field Testing Facility. *AIMS Geosci* 5: 509–534. https://doi.org/10.3934/geosci.2019.3.509
18. Massop HTL, Hessel R, van den Akker JJH, et al. (2024) Monitoring long-term peat subsidence with subsidence platens in Zegveld, the Netherlands. *Geoderma* 450: 117039. https://doi.org/10.1016/j.geoderma.2024.117039
19. Landva AO (2007) Characterisation of Escuminac peat and construction on peatland. In: Tan TS, Phoon KK, Hight DW, et al. Eds., *Characterisation and Engineering Properties of Natural Soils*, Taylor& Fransic Group London, 2135–2191.
20. Hobbs NB (1986) Mire morphology and the properties and behaviour of some British and foreign peats. *Q J Eng Geol Hydrogeol* 19: 7–80. https://doi.org/10.1144/GSL.QJEG.1986.019.01.02
21. Konstadinou (2024) Effect of cyclic preloading on the generation of excess pore water pressure and strain accumulation for cohesive soils, experimental testing for RESET factual report, Deltares report nr 11208747–003.
22. Deltares, TKI verbeteren zettingsprognose, incremental loading oedometer tests Zegveld NOBV, Deltares report nr 11203922–004–GEO–0003. 2021.
23. NEN, NEN-EN-ISO 17892-5. Geotechnical investigation and testing—Laboratory testing of soil—Part 5: Incremental loading oedometer test. Delft, the Netherlands, 2017. Available from: https://www.nen.nl/.
24. Den Haan EJ, Kruse GAM (2007) Characterisation and engineering properties of Dutch peats. *Characterisation and Engineering Properties of Natural Soils*, London Taylor & Francis, 3: 2101–2133.

25. Mesri G, Ajlouni M (2007) Engineering properties of fibrous peats. *J Geotech Geoenviron Eng* 133: 850–866. https://doi.org/10.1061/(ASCE)1090-0241(2007)133:7(850)
26. Casagrande A, Fadum RE (1940) Notes on soil testing for engineering purposes. Harvard Graduate School of Engineering.
27. ASTM Committee D-18 on Soil and Rock, *Standard Test Methods for One-Dimensional Consolidation Properties of Soils Using Incremental Loading*, ASTM International West Conshohocken, USA. 2011.
28. Noorlandt R, Drijkoningen G, Dams J, et al. (2015) A seismic vertical vibrator driven by linear synchronous motors. *Geophysics* 80: 57–67. https://doi.org/10.1190/geo2014-0295.1
29. Lunne T, Powell JJM, Robertson PK (2002) *Cone Penetration Testing in Geotechnical Practice*, CRC Press.
30. Robertson PK, Cabal KL (2010) Estimating soil unit weight from CPT. *2nd International symposium on cone penetration testing*, California, USA: Gregg Drilling & Testing Inc, 2–40.
31. Lengkeek A (2024) CPT based classification with focus on organic soils. *7th International Conference on Geotechnical and Geophysical Site Characterisation*, Barcelona, 18–21. https://doi.org/10.23967/isc.2024.154
32. NEN, NEN EN-ISO 22476-1:2012, IDT Geotechnical investigation and testing—Field testing—Part1: electrical cone and piezocone penetration test. Delft, the Netherlands, 2013. Available from: https://www.nen.nl/.
33. Rijkswaterstaat, Schematiseringshandleiding macrostabiliteit (Version 4.0). Ministerie van Infrastructuur en Milieu. In Dutch. 2021. Available from: https://iplo.nl/@205756/schematiseringshandleiding-macrostabiliteit/.
34. Schneider JA, Randolph MF, Mayne PW, et al. (2008) Analysis of factors influencing soil classification using normalized piezocone tip resistance and pore pressure parameters. *J Geotech Geoenviron Eng* 134: 1569–1586. https://doi.org/10.1061/(ASCE)1090-0241(2008)134:11(1569)
35. Vesterberg B, Mattias A, Burman F, et al. (2025) CiPPT—A new in situ method for sounding and strength determination in peat. *AIMS Geosci* 11: 558–576. https://doi.org/10.3934/geosci.2025024
36. Terzaghi K (1943) *Theoretical soil mechanics*, John Wiley & Sons, Inc., New York.
37. Biot MA (1941) General theory of three-dimensional consolidation. *J Appl Phys* 12: 155–164. https://doi.org/10.1063/1.1712886
38. Zhang WW, Zhu G, Wang R, et al. (2009) Solution charts for the consolidation of circular footings embedded in a finite stratum. *Can Geotech J* 46: 708–718. https://doi.org/10.1139/T09-005
39. Georgiadis K (2010) Undrained Bearing Capacity of Strip Footings on Slopes. *J Geotech Geoenviron Eng* 136: 677–685. https://doi.org/10.1061/(ASCE)GT.1943-5606.0000269
40. Houlsby GT, Martin CM (2003) Undrained bearing capacity factors for conical footings on clay. *Geotechnique* 53: 513–520. https://doi.org/10.1680/geot.53.5.513.37507